

Simulation of multiple supra-arcade downflows in solar flares

M. Cécere^{1,2}, M. Schneider^{1,3,4}, A. Costa^{1,3,4}, S. Elaskar^{1,4} and S. Maglione⁵

ABSTRACT

In later papers we have shown that sunward, generally dark, plasma features originated above posteruption flare arcades are consistent with a scenario where plasma voids are generated by the bouncing and interfering of shocks and expansion waves upstream of an initial localized deposition of energy which is collimated in the magnetic field direction. In this paper we analyze the multiple production and interaction of supra-arcade downflows (SAD) and the structure of individual SADs that make them relatively stable features while moving. We compare our results with observations and with the scenarios proposed by other authors.

Subject headings:

1. Introduction

Sunward dark moving trails with origin [40 – 60]Mm above posteruption flare arcades and decelerating speed in the range $\sim [50 - 500]\text{km s}^{-1}$ were first detected with the *Yohkoh* Soft X-ray Telescope (SXT). Since then, they have been extensively reported using other instruments such as *TRACE* (Innes et al. 2003a,b), *SOHO/SUMER* (Innes et al. 2003b) and *SDO/AIA* (Savage et al. 2012). The lack of X-ray and extreme-ultraviolet (EUV) signatures in images and spectra has led to consensus on that these down-moving structures ought to be voided flows generated by reconnection processes in a current sheet above the flare arcade. Besides the dark moving structures, bright supra-arcade downflowing features have also been reported during flares (McKenzie 2000).

McKenzie and Savage (2009), Savage and McKenzie (2011) suggested that supra-arcade downflows (SAD) are the cross-sections of thin and empty flux tubes retracting from a reconnection site high in the corona.

According to these authors, the high enough inner magnetic pressure could be the reason the voids are able to resist being filled in immediately by the surrounding denser plasma. Linton et al. (2009) proposed a scenario where the dynamic of retracting magnetic fields is triggered by a localized reconnection event that produces up and down flowing reconnected flux tubes, which are slowed down by underlying magnetic arcade loops. The observed SAD speeds are lower than expected for reconnection outflows in regions of typical Alfvén speeds of 1000 km s^{-1} . Linton et al. (2009) suggested that drag forces could work against the reconnection outflow.

Verwichte et al. (2005) analyzed TRACE SAD oscillations transverse to the magnetic field. They found that the initial speeds and the displacement amplitudes, of kink-like type in the observational dark lanes of variable sizes (between $[\sim 2 - 9]\text{Mm}$), decrease as they propagate downwards, while the period remains fairly constant with height.

Recently, after AIA observations with high resolution and cadence, Savage and McKenzie (2011) re-interpreted SADs as wakes created by the retraction of thin loops instead of the previous interpretation as flux tube cross-sections (renamed by the authors as SADLs). They interpreted SADLs as features of sizes $[\sim 0.9 - 1.3]\text{Mm}$ observed during the early phase of the eruptive event and SADs as features of sizes $\sim 9\text{Mm}$ that become apparent afterwards. They proposed that deceleration is expected due to the buildup of down-

¹Consejo Nacional de Investigaciones Científicas y Técnicas (CONICET), Argentina.

²Facultad de Matemática, Astronomía y Física, Universidad Nacional de Córdoba (UNC), Córdoba, Argentina

³Instituto de Investigaciones en Astronomía Teórica y Experimental IATE, Córdoba, Argentina.

⁴Facultad de Ciencias Exactas, Físicas y Naturales, Universidad Nacional de Córdoba (UNC), Córdoba, Argentina

⁵Facultad de Ingeniería, Universidad Nacional de Río Cuarto, Ciudad Universitaria, Río Cuarto, Córdoba, Argentina

stream magnetic pressure and/or drag mechanisms.

In Costa et al. (2009), Schulz et al. (2010) and Maglione et al. (2011) (hereafter Paper 1–3, respectively) we showed, by means of 1 and 2D MHD simulations, that the dark tracks are consistent with plasma voids generated by the bouncing and interfering of shocks and expansion waves upstream of the initial localized deposition of energy. The composition of both, a resulting sunward directed hydrodynamic shock pattern and a perpendicular magnetic shock produce an overall transversely shaking void that propagates towards the surface of the sun, resembling the kink-like mode described in Verwichte et al. (2005). Contrary to the 1D results –where the sunwards dynamic is independent on the magnetic field intensity owing to its exclusive waveguide role– in the 2D simulation the sunwards speed is higher for higher values of the magnetic field. This can be interpreted as the capability of the low coronal plasma to collimate the deposition of energy in the magnetic field direction.

As we obtained larger inner values of β than outer the voided cavity (see Fig. 2 of Paper 2), with the contour in total pressure equilibrium with the environment, we concluded that the internal magnetic pressure cannot be responsible of preventing the collapse of the vacuum zone. Instead, we found that the higher values of β inside the SADs are due to hotter plasma concentrated in regions of $T > 20$ MK (Warren et al. 1999), which are consistent with the observations, despite the low inner values of density.

We concluded that the voids seem to be emergent structures of a whole nonlinear interacting plasma context of shocks and waves that upwardly rebound resembling the reconnection site, are absorbed sunwardly, and rebound in the lateral denser medium, instead of voided plasma loops that are magnetically structured.

In this paper, in the frame of Paper 1–3’s scenario –where reconnection is required to provide the energy deposition that triggers the phenomenon but not to give account of the shape, the sizes, the thermodynamic parameters and the SADs dynamic– and with the aim of testing the scopes of our model, we focus on reproducing the dynamic and interaction of multiple of these voided structures. In Paper 1–3 we found that to reproduce the oscillating pattern we required closed boundary conditions. However, in Paper 2 we found that the oscillating pattern was robust under a broad variation of the boundary conditions –contemplating different density values at the extremes and allowing

total or partial boundary rebounds. Thus, the question arises about the role played by the boundary conditions. The observations show that the dark lanes sustain their individual configuration all the way down into the arcade structure. Thus, the simulation of multiple lanes triggered by different pressure pulses must maintain these individualities while they evolve decelerating sunwardly. However, can we consider the dynamic of a multiple dark lane structure as the superposition of individual dark lanes (as described in Paper 1–3)? If this is the case, what produces the wavy features described in Verwichte et al. (2005)?

2. Numerical code and initial conditions

We carried out the 2D-MHD-simulations with the Mezcal code, which has been extensively tested in several scenarios (see for instance De Colle and Raga (2006) or De Colle et al. (2008)). All calculations were performed with a numerical grid of $(x, y) = (400, 800)$ grid-points and a physical size of $(20, 40)$ Mm, corresponding to a resolution of $(50, 50)$ km. The coordinate y represents the sunwards direction and the x coordinate the transverse to the magnetic field one. We assumed a constant radial initial magnetic field structure, and typical background temperature of $T = 1.0 \times 10^6$ K. Simultaneous ($t = 0$ sec) spherical pulses $(\Delta P/P)_i = (110, 90, 110)$ $i = 1, 3$ (ΔP is the triggering pressure pulse and P is the background gas pressure of the corona) of a radius 0.6Mm were localized in positions $(67, 720)$, $(167, 680)$ and $(333, 720)$ corresponding to $(3.35, 36.0)$ Mm, $(8.35, 34.0)$ Mm and $(16.65, 36.0)$ Mm, respectively.

Several simulations were carried out, varying the magnetic field, B and the density ρ . Also, we added a localized deposition of energy -modeled as a new triggering pressure pulse, $(\Delta P/P)_4$ - resembling a new reconnection event (at $t = 200$ sec) occurring in the scenario modified by the later ones. Table 1 shows the different models used for the simulations. We employed open or non-reflecting conditions for the lateral boundaries, whereas only a fix rebound condition was used at the upper radial direction, resembling the action of the reconnection site, and transmission condition for the bottom boundary, assuming that the perturbations are absorbed in the sunwards direction. The characteristic boundary parameters were chosen in accordance with typical observed dark lane structures, as in Verwichte et al. (2005) and McKenzie and Hudson (1999).

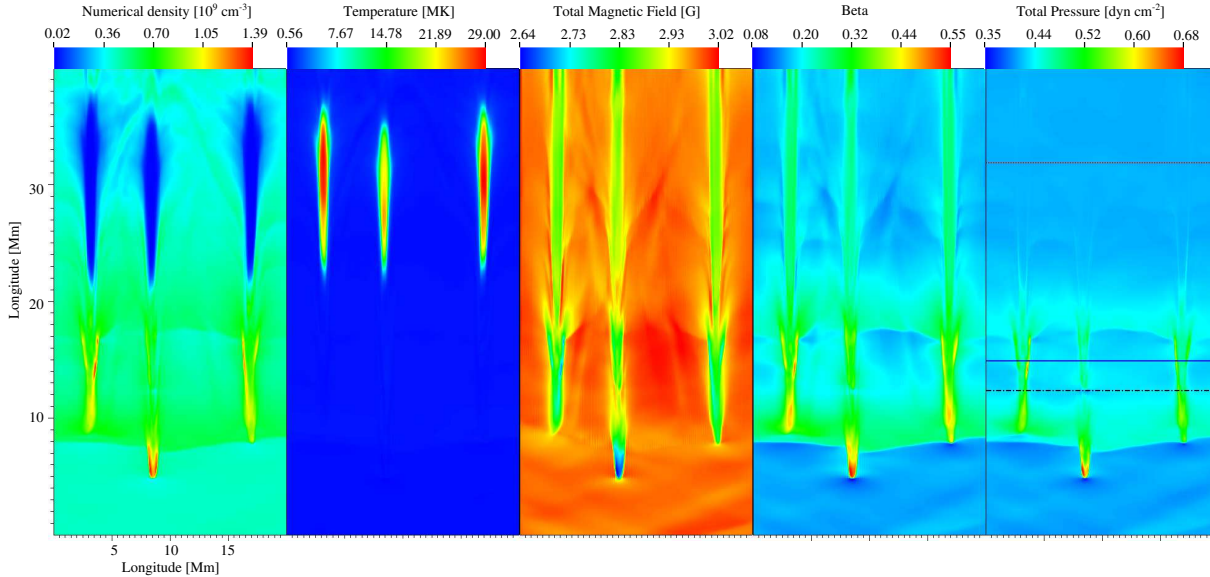


Fig. 1.— Simulation, at $t = 196\text{sec}$, of: a) density, b) temperature, c) total magnetic field d) β -parameter and e) total pressure of the three SADs.

3. Results and Discussion

Are the lane dynamics independent one from the other one? Figure 1 shows, the $M1$ evolution of the three voided features at $t = 196\text{sec}$, it simulates, respectively, the voided density tracks left by three simultaneous reconnection bursts, the temperature, the magnetic field, the β -parameter and the total pressure for open boundary conditions. From Fig. 1a we see that, as expected (e.g. McKenzie and Hudson (1999)) the vacuum density values are less than the environment ones in more than one order of magnitude (see the features above $y = 20\text{Mm}$); the temperature (Fig. 1b) is more than one order of magnitude higher in the voided cavities than outside (as in Longcope et al. (2009), Warren et al. (1999)); the inner magnetic field is lower than its external value ($< 1\text{G}$) (Fig. 1c), thus, the inner magnetic pressure cannot be responsible of preventing the collapse of the vacuum zone. The β -parameter (Fig. 1d) is larger inside than outside. Furthermore, from the upper part of Fig. 1e we can see that the total pressure of the region is almost constant, i.e., the features that characterize the vacuum zone have disappeared, meaning that the contour of the cavity is, on average, in total pressure equilibrium, as in Paper 3.

The multiple SAD dynamics reproduces the individual dynamic; i.e., in accordance with observational

data, the temporal evolution analysis gave us decelerating SADs speeds of the order of $100 - 300\text{km s}^{-1}$. The freezing-in of the plasma to the magnetic field induces the collimation of most of the kinetic energy towards the longitudinal direction, which is enhanced with the increase of the magnetic field. In accordance with Paper 3 (see Table 1 of the paper) –where we obtained a slow increase in the initial speed with the increase of the background magnetic field– for a run of 200sec , varying the magnetic field from 3G to 10G (models $M1$ and $M2$) the distance evacuated by the perturbation increases 4Mm ; while varying the background numerical density from $0.46 \cdot 10^9\text{cm}^{-3}$ to $3 \cdot 10^9\text{cm}^{-3}$ (models $M2$ and $M3$) the distance evacuated by the perturbation diminishes in 6Mm . Thus, the void dynamics in multiple events must be sustained by the interaction of localized (confined to the individual dark tracks) nonlinear waves and shocks acting in times comparable to the observations (see Paper 3).

In the bottom region of Fig. 1, e.g., $y \sim 10\text{Mm}$, we note an increase of the density (Fig. 1a), the β -parameter (Fig. 1d) and the total pressure (Fig. 1e) with respect to their corresponding background values; correspondingly we note a decrease of the magnetic field (Fig. 1c). These bottom overdense tear-shaped features can be associated with the bright downward features described by McKenzie (2000). In our scenario, bright SADs are the shock fronts that open the

way towards the sun surface. In accordance with the observational fact that bright SADs are not as commonly observed as dark SADs, the simulated voided dark tracks are larger and more elongated than the bright fronts.

As in the simulations with a single SAD, the multiple structures produce temporal patterns which remind observational constrictions (Innes et al. 2003a), (Innes et al. 2003b), see the knots in the SAD traces of Fig. 1. These constrictions were interpreted as a bursty production in the reconnection scenario proposed by Linton et al. (2009) and Savage and McKenzie (2011). In our results these patterns are obtained as a result of the nonlinear shock dynamic. Figure 2 shows the total pressure at the heights indicated with cuts in Fig. 1e: ~ 32 Mm, ~ 15 Mm and ~ 12 Mm. Note that the total pressure is fairly constant in the upper region, near the triggering site at ~ 32 Mm (dotted line). At ~ 15 Mm, (solid line) the total pressure is higher inside the tracks. The constrictions or knots (e.g see the second SAD at ~ 12 Mm, dashed–dotted line) correspond to regions of total internal pressure lower than the outside values.

As shown in Fig. 1, in accordance with what is expected from observations, it appears that dark lanes are not distorted by the fact that they are multiple. There is not an appreciable evidence of the interaction between SADs. Savage and McKenzie (2011), in the frame of the scenario proposed by Linton et al. (2009), interpreted the discreteness of SADs as an indication that the reconnection is highly localized. In our scenario, as in the one proposed by Linton et al. (2009), the production of plasma voids are associated with reconnection bursts, but we do not assume a 2D configuration nor a particular magnetic topology of the current sheet (Priest and Démoulin 1995). The scenario proposed by Linton et al. (2009) relates inherently the plasma voids to reconnections that occur within the current sheet. In our case reconnection is not modeled but simulated as a pressure pulse that triggers the void pro-

Model	$B[G]$	$n * 10^9[cm^{-3}]$	$(\Delta P/P)_4$
<i>M1</i>	3	0.46	400
<i>M2</i>	10	0.46	400
<i>M3</i>	10	3	400
<i>M4</i>	3	0.46	200

Table 1: Simulated models: \vec{B} the background magnetic field in the radial direction, ρ the background density.

duction in a homogeneous media. Thus, we can still be concerned about the extent of the independent behavior between different SADs.

An indication of the interaction between SADs seems to be the wavy appearance that can be seen in some observations, e.g. Verwichte et al. (2005). There is an important difference between 1D and 2D simulations in relation with the ability to generate the kink–like appearance of the SADs. In Papers 1-2 (1D simulations) the kink–like features are simply obtained due to lateral rebounds that emulate a neighbor denser medium (see Fig. 2 and Fig. 1 of Paper 1 and 2 respectively). The oscillatory pattern is sustained over time and the wave structure does not lose energy. In Paper 3 (2D), the wavy appearance of a lateral cut is damped in few periods (see Fig. 1a of that paper), but if we focus in the 2D slides (see Fig. 2 of Paper 3) it is not possible to recognize the wavy character. It seems that the spatial distribution of energy of the 2D lateral rebounds (with closed boundary conditions) leads to a rapid damping of the oscillations and would not give account of the wavy appearance of the observations.

Meanwhile, comparing the evolution of nonlinear waves produced by a triggering pressure pulse in the 1D and 2D cases we recognize a similar dynamic behavior that prevails during time and could explain the robustness of the voided patterns. Figure 3a shows the spontaneous 1D non–dimensional density evolution due to the action of a pressure pulse over a medium with static initial condition (Fernández et al. 2009). In Figure 3b the triggering pulse is asymmetrically located, as in our runs.

A detailed description of the evolution of the voided features can be obtained from these figures and from the wave analysis provided by the numerical techniques used. Figure 3a displays nondimensional time step numbers 200, 800, and 2000. Time step 0 corresponds to $\rho(0) = 1$. In the figure we see two shock wave fronts for each time step, e.g., for step 800, the shocks are located at $(x_{1s} = 39; x_{2s} = 111)$ Mm. Also, for the same time step two contact discontinuities are found at $(x_{1c} = 46.5; x_{2c} = 103.5)$ Mm and two expansion waves are found starting at $(x_{1e} = 57; x_{2e} = 93)$ Mm. Initially two shock fronts moving away from the triggering pressure pulse location are formed (see e.g. time step 200 in Fig. 3a and Fig. 3b). As the shocks travel along the magnetic field direction, the temperature and the density are increased making the energy rise, e.g. $(x_{1s} = 39; x_{2s} = 111)$ Mm in time step 800 of Fig. 3a. The density is abruptly diminished (e.g.

($x_{1c} = 46.5$; $x_{2c} = 103.5$)Mm in time step 800) by contact discontinuities that go behind the shocks and can be recognized because the pressure and the velocity of the flow are not changed while the waves pass. The temperature increases to maintain a constant pressure across the contact discontinuities. Also, two expansion waves –that are recognized because they diminish the density while they pass– are initially produced and travel towards the triggering position, contrary to the shock fronts (e.g. ($x_{1e} = 55.5$; $x_{2e} = 94.5$)Mm at time step 200 in Fig. 3a). These waves collide, rebound at the triggering location (see Fig. 3a–b, center part for time steps 800), and then travel in the opposite direction towards the contact discontinuities (e.g. ($x_{1e} = 57$; $x_{2e} = 93$)Mm of time step 800 in Fig. 3a). From the comparison of time step 800 and time step 2000, we see that the expansion waves have a larger speed than the contact discontinuity. At time step 2000 the position of the shock fronts in Fig. 3a are ($x_{1s} = 7.5$; $x_{2s} = 142.5$)Mm, the expansion waves have interacted with the contact discontinuities and lowered the density and pressure leaving behind a coupled nonlinear system of waves, e.g., the ranges ($\Delta x_1 = 31.5 - 7.5$; $\Delta x_2 = 142.5 - 118.5$)Mm in Fig. 3a and ($\Delta x_1 = 28.5 - 15.0$; $\Delta x_2 = 109.5 - 91.5$)Mm in Fig. 3b. As a result of this dynamic a central voided cavity, which we call SAD, is formed.

Figure 3c, shows a 2D density cut taken along the SAD located at $x = 19$ Mm in Fig. 1a. The similarity between Fig. 3a–b and Fig. 3c (compare $t = 8$ sec in Fig. 3c with time step 800 in Fig. 3a–b and $t = 180$ sec in Fig. 3c with time step 2000 in Fig. 3a–b) expresses the likeness between the dynamic behavior of the 1D and 2D descriptions. There are, however, small differences in the shape of Fig. 3c at $t = 180$ sec from the ones in Fig. 3a–b, time step 2000. Comparing the features ranging from $x = (10-20)$ Mm in Fig. 3c with the corresponding features in Fig. 3a–b, we note that even when the patterns are similar the more irregular shape in Fig. 3c can be attributed to perturbations produced by the other SADs.

However, we found cases where the interaction between SADs is evident and has the observational consequence that it reproduces the wavy SAD character registered by Verwichte et al. (2005). Figure 4a–b shows the SAD evolution for $M1$ after a new pressure pulse, triggered at $t = 200$ sec, has developed a wavefront over the discrete tracks left by the three initial SADs that have traveled decelerating a distance of ~ 16 Mm (Fig. 4a). In the upper part of Fig. 4b

at $t = 300$ sec it appears that the initial SADs have lost their discreteness. We have stated that when the magnetic field is uniform the energy produced by the pressure pulse is distributed in a non–homogeneous way due to the collimation generated by the magnetic field. While the SADs propagate further a new trace left by the new burst can be seen sunwards (Fig. 4b). Also, the new reconnection pulse injects energy most of which is distributed in a non–uniform way between the wakes left by the previous SADs i.e., the initially spherical pressure pulse (Fig. 4a) at 212sec is later collimated by the magnetic field configuration at 300sec (Fig. 4b). As in the other cases, the sunward elongation of the fourth lane is due to the interaction of upper rebounds and downward absorptions along the magnetic field that collimates the flow.

A remarkable effect which has observational implications is the distribution of kinetic energy. As can be seen from Fig. 5a, part of the new SAD kinetic energy is distributed along the wakes left by the previous SADs. In accordance with the observations, when the sequence is seen as a movie the wakes exhibit a wavy motion (e.g. (Verwichte et al. 2005), (McKenzie 2000), (Khan et al. 2007)). This can be explained due to the tendency of the wavefront energy to deviate into lower density regions, i.e., the wakes left by the previous SADs. The continuity Rankine–Hugoniot relation for hydrodynamic shocks, i.e., the shock in the longitudinal direction (Paper 1–3), and in the shock wave frame is

$$v_u = \frac{\rho_d}{\rho_u} v_d \quad u \text{ upstream, } d \text{ downstream.}$$

Initially, the energy of the pressure pulse is almost spherically distributed due to its larger pressure value with respect to the ambient one (Fig. 4a), so we can consider that ρ_d and v_d are almost the same all around the spherical boundary of the initial shock front. However, the corresponding upstream ρ_u values will be different depending on the previous SAD distribution, i.e., ρ_u is almost an order of magnitude lower in the wakes left by the previous SADs. Thus, initially the upstream flow speed will be larger in the SAD wakes than in the neighbor ambient. Moreover, the previous SADs have larger values of the flow speed than the ambient one and its value will be added to the upstream speed. This implies that two upstream shock front positions with initial values $\rho_A < \rho_B$, and thus $v_A > v_B$, will continue their motion with $v_A > v_B$ while the shock wave travels. Obviously, the same relation stands for the kinetic energy, i.e. $K_A = \rho_A v_A^2 =$

$\rho_B v_B v_A > \rho_B v_B^2 = K_B$ (K the kinetic energy). Upstream, this relation is preserved as can be appreciated in Fig. 5a. Compare the kinetic energy of A and B in this figure with their corresponding densities ($\rho_A < \rho_B$) in Fig. 4b. Note the correspondence between the low–high density values in positions A and B in Fig. 5a with respect to the high–low kinetic energy values in the same positions in Fig. 4b. The energy of the fourth reconnection event is partly deviated from the new wake into the previous ones depending on the background plasma parameter. Figure 5b shows the kinetic density energy for $M2$ at $t = 300\text{sec}$. When the magnetic field intensity is increased (or the intensity of the pressure pulse is diminished, model $M4$) the wavy character is lost.

This description could also explain the difference between SADs and SADLs described by Savage and McKenzie (2011). From Fig. 4b it is evident that due to the second pulse we can attribute different sizes to the SADs, depending on the effect produced by the new wavefront in the medium, this can also be noted from the kink–like structures in Verwichte et al. (2005). The features of size [$\sim 0.9 - 1.3$]Mm described as SADs by Savage and McKenzie (2011) can be associated with our first SADLs, while the features of size [~ 9]Mm described as SADs by Savage and McKenzie (2011) with our new SAD. Moreover, our description in terms of features that firstly elongate straight towards the sun and later approach waiving the sun surface are in tuning with the observations described in Savage and McKenzie (2011), i.e., the smaller structures (seen during the early phase) tend to travel straight down, while the larger ones (seen afterwards, when there is a significant increase of hot plasma) approach the arcade from an angle.

4. Conclusions

We analyze the dynamic of multiple dark supra-arcade lanes that move decelerating towards the sun surface. In the scenario we proposed, dark lanes are explained as the evolution of shocks and expansion waves that form confined voided cavities –of high temperature and β values– collimated in the direction of the ambient magnetic field. These features sustain their morphology over time behaving as a whole pattern (almost independently from boundary conditions and other perturbations) with a sunward and decelerating motion triggered by upward reconnection events. We found that the less common observational bright

SADs could be interpreted as the bottom overdense tear-shaped features forming shock fronts that open the way towards the sun surface. In our scenario, the different observational sizes distinguished as SADLs and SADs by Savage and McKenzie (2011) could be interpreted as reconnection events that are triggered in a background homogeneous media or as reconnection events triggered in a background media with previous SAD formations, respectively.

When multiple SAD configurations are analyzed we note that the wave structure of each SAD is similar to the individual pattern reinforcing the non-interacting hypothesis. However, we found that the wavy character that can be seen in some observations can be interpreted as an indication of interaction between SADs. This interaction is significative when the bursts that trigger the phenomenon act over the wakes left by previous SADs. This wavy character is enhanced with the strength of the reconnection and/or with lower values of the magnetic field intensity.

REFERENCES

- Costa, A., Elaskar, S., Fernández, C. A., and Martínez, G. (2009). Simulation of dark lanes in post-flare supra-arcade. *MNRAS*, 400:L85–L89.
- De Colle, F. and Raga, A. C. (2006). MHD simulations of radiative jets from young stellar objects. $\text{H}\alpha$ emission. *A&A*, 449:1061–1066.
- De Colle, F., Raga, A. C., and Esquivel, A. (2008). The Dynamics of Internal Working Surfaces in Magnetohydrodynamic Jets. *ApJ*, 689:302–307.
- Fernández, C. A., Costa, A., Elaskar, S., and Schulz, W. (2009). Numerical simulation of the internal plasma dynamics of post-flare loops. *MNRAS*, 400:1821–1828.
- Innes, D. E., McKenzie, D. E., and Wang, T. (2003a). Observations of 1000 km s^{-1} Doppler shifts in 10^7 K solar flare supra-arcade. *Sol. Phys.*, 217:267–279.
- Innes, D. E., McKenzie, D. E., and Wang, T. (2003b). SUMER spectral observations of post-flare supra-arcade inflows. *Sol. Phys.*, 217:247–265.
- Khan, J. I., Bain, H. M., and Fletcher, L. (2007). The relative timing of supra-arcade downflows in solar flares. *A&A*, 475:333–340.

- Linton, M. G., Devore, C. R., and Longcope, D. W. (2009). Patchy reconnection in a Y-type current sheet. *Earth, Planets, and Space*, 61:573–576.
- Longcope, D. W., Guidoni, S. E., and Linton, M. G. (2009). Gas-dynamic Shock Heating of Post-flare Loops Due to Retraction Following Localized, Impulsive Reconnection. *ApJL*, 690:L18–L22.
- Maglione, L. S., Schneiter, E. M., Costa, A., and Elaskar, S. (2011). Simulation of dark lanes in post-flare supra-arcades. III. A 2D simulation. *A&A*, 527:L5.
- McKenzie, D. E. (2000). Supra-arcade Downflows in Long-Duration Solar Flare Events. *Sol. Phys.*, 195:381–399.
- McKenzie, D. E. and Hudson, H. S. (1999). X-Ray Observations of Motions and Structure above a Solar Flare Arcade. *ApJL*, 519:L93–L96.
- McKenzie, D. E. and Savage, S. L. (2009). Quantitative Examination of Supra-arcade Downflows in Eruptive Solar Flares. *ApJ*, 697:1569–1577.
- Priest, E. R. and Démoulin, P. (1995). Three-dimensional magnetic reconnection without null points. 1. Basic theory of magnetic flipping. *J. Geophys. Res.*, 100:23443–23464.
- Savage, S. L. and McKenzie, D. E. (2011). Quantitative Examination of a Large Sample of Supra-arcade Downflows in Eruptive Solar Flares. *ApJ*, 730:98.
- Savage, S. L., McKenzie, D. E., and Reeves, K. K. (2012). Re-interpretation of Supra-arcade Downflows in Solar Flares. *ApJL*, 747:L40.
- Schulz, W., Costa, A., Elaskar, S., and Cid, G. (2010). Simulation of dark lanes in post-flare supra-arcades - II. A contribution to the remote sensing of the coronal magnetic field. *MNRAS*, 407:L89–L93.
- Verwichte, E., Nakariakov, V. M., and Cooper, F. C. (2005). Transverse waves in a post-flare supra-arcade. *A&A*, 430:L65–L68.
- Warren, H. P., Bookbinder, J. A., Forbes, T. G., Golub, L., Hudson, H. S., Reeves, K., and Warshall, A. (1999). TRACE and Yohkoh Observations of High-Temperature Plasma in a Two-Ribbon Limb Flare. *ApJL*, 527:L121–L124.

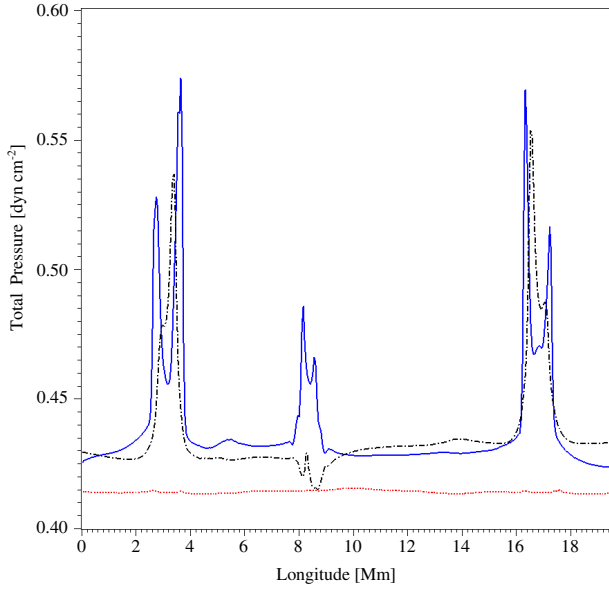


Fig. 2.— Total pressure of the three SADs at $t = 196\text{sec}$ and heights: 32Mm (dotted line), 15Mm (solid line) and 12Mm (dashed-dotted line). See the constriction located at 12Mm in the second SAD.

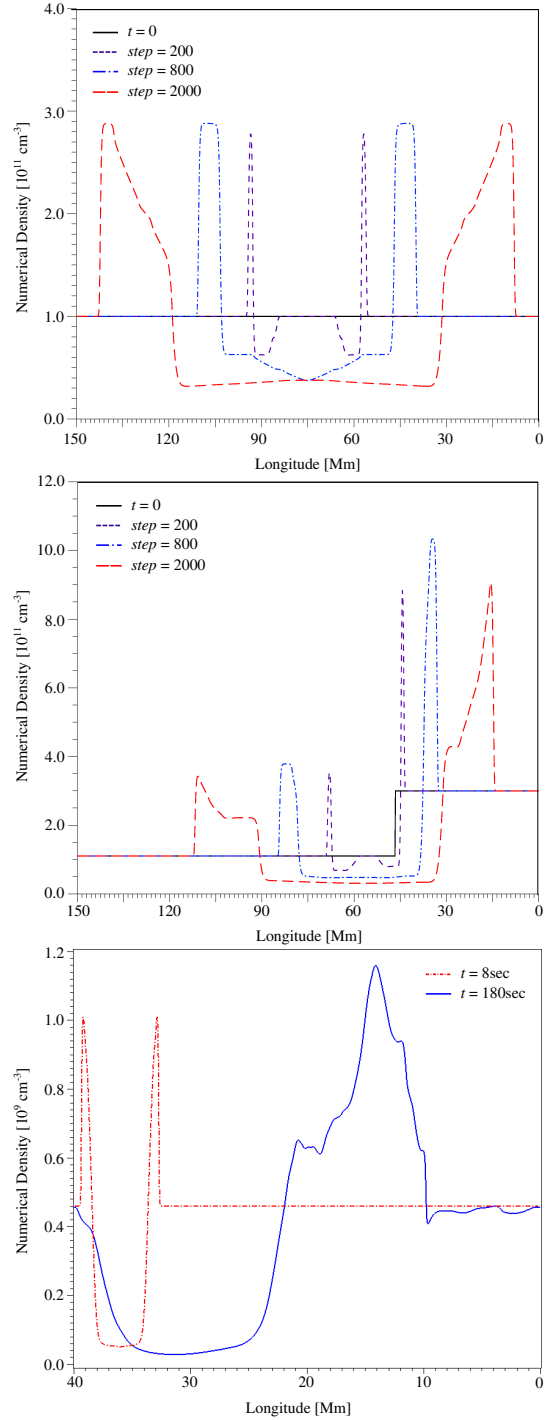


Fig. 3.— Upper panel) 1D density evolution after a central triggering pressure pulse for different time steps, Middle panel) 1D density evolution after an asymmetric triggering pressure pulse for different time steps, Lower panel) 2D SAD density evolution for a cut at $x = 19\text{Mm}$ in Fig. 1a.

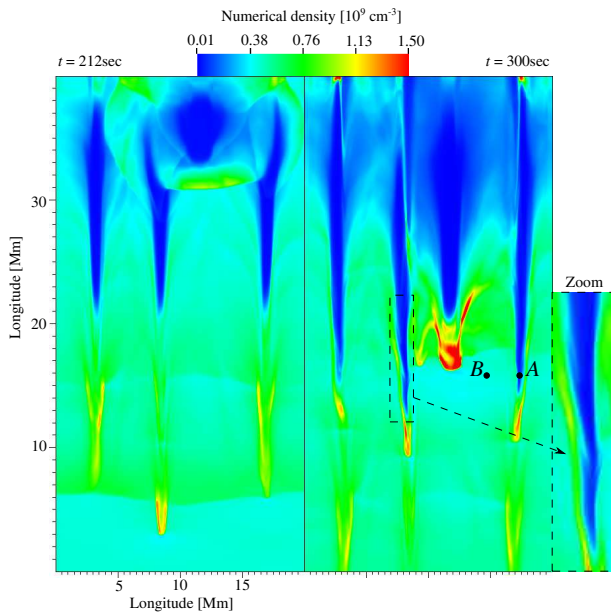


Fig. 4.— $M1$ numerical density after a fourth pressure pulse, the event is seen at left) $t = 212\text{sec}$, and at right) $t = 300\text{sec}$. Note the wavy features (zoom) due to the interaction between SADs.

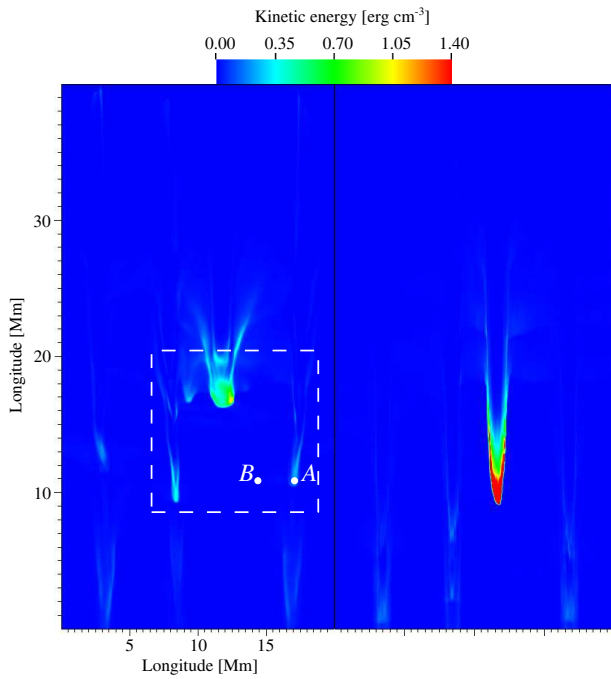


Fig. 5.— Kinetic density energy collimated into the wakes left by previous SADs; left) $M1$ at $t = 300\text{sec}$, and right) $M2$ at $t = 300\text{sec}$.